Journal of Materials and Environmental Science
ISSN : 2028-2508
CODEN : JMESCN

J. Mater. Environ. Sci., 2020, Volume 11, Issue 7, Page 1173-1183

http://www.jmaterenvironsci.com

Mineralogical characterization of Upper Cretaceous petroleum source rocks of Termit sedimentary basin (Niger)

M. B. Alassane Ibrahim [1], K. A. Yao [1*], Z. B. Digbehi [2]

[1]Laboratoire de Génie Civil, Géosciences et Sciences Géographiques, Institut National Polytechnique Félix Houphouët-Boigny, de Yamoussoukro BP 1093, Côte d'Ivoire
[2]Biostratigraphie et Sédimentologie, UFR-STRM, Université Félix Houphouët-Boigny, Abidjan/Côte d'Ivoire

Received 22 May 2020,
Revised 25 June 2020,
Accepted 27 June 2020

Keywords
- ✓ Termit Basin,
- ✓ mineralogical characterization,
- ✓ XRD,
- ✓ infrared,
- ✓ FRX.

alphonse.yao@inphb.ci
Phone: +22588914364

Abstract

The Dg and Yg source rocks of Termit sedimentary basin were subjected to mineralogical characterization to determine if they present a risk of swelling. Mineralogy is determined by X-ray diffraction on crude rocks and clayey fractions. It is mainly dominated by clay (52.80% for Dg and 42.70% for Yg), quartz (25.20% for Dg and 32.60% for Yg) and a significant proportion of muscovite (5,00% for Dg and 8,84% for Yg) and pyrite (12,80% for Dg and 7,00% for Yg). The clayey fractions are dominated by kaolinite (51.00 and 67.9%) and have interstratified minerals at two and three sheets. These interstratified are composed of illite-smectite (31.40%) and illite-chlorite (17.60%) for Dg and illite-smectite-chlorite (32.10%) for Yg. These results are verified by X-ray fluorescence spectroscopy and scanning electron microscopy on crude rocks and then confirmed by infrared spectrometry. The specific surface areas of these clays determined by BET, are respectively 530.40 m 2 / g and 464.90 m 2 / g for Dg and Yg. In total, the mineralogical composition of the crude rocks and their clayey fractions analyzed as well as their specific surface areas show that these rocks present a risk of swelling.

1. Introduction

Upper Cretaceous petroleum source rocks (Yg and Dg formations) of Termit sedimentary basin (Niger) are mainly composed of clays. These clays have been the subject of several studies, including mineral and organic petrography, organic geochemistry and paleontology [1–9] to determine the level of thermal maturity, characterize the depositional environment, and evaluate their oil potential. Other studies have focused on the characterization of the basin's oil reservoirs [10–17].

The interest of clays study in general and clay minerals in particularly, is based on their multiple applications as water treatment materials, paint components, barriers against pollutants, adsorbent substances, catalysts and as drilling fluids [18–22]. Other studies determined the behaviour of some clay minerals to prevent the risk of shrinkage and swelling of clays [23–25]. This phenomenon of shrinkage and swelling is very common in oil drilling operations because the role of mud-cake is predominant for porous and permeable formations [26]. Knowledge of mineralogical composition of these clay source rocks will determine if they present a risk of swelling, a phenomenon that causes jamming of drilling rig and drilling bit.

Therefore, this work focuses on mineralogical characterization of Dg and Yg clay formations, which may be crossed by oil exploration and development drilling in Termit sedimentary basin.

2. Material and Methods

2.1 Study area

The Mesozoic and Cenozoic intracontinental Termit basin is a sub-basin of Eastern Niger sedimentary basin which is located between parallels 14°15 and 17° northern latitude and meridians 14° and 11°45 western longitude. It is limited in Niger by two major geological areas. From the west and northwest, the basin is bordered by crystalline rocks from basement of Gouré Precambrian massif and Zinder Mesozoic massif (Damagaram Mounio), in the north by Téfidet basin and Ténéré basin (Fig 1) and in the east and northeast by of Dibella Mesozoic granite [9]. In the south, the Termit basin is bordered by the Bornu basin at the northern boundary of northern zone for Benoue faults in Nigeria and Chad [6].

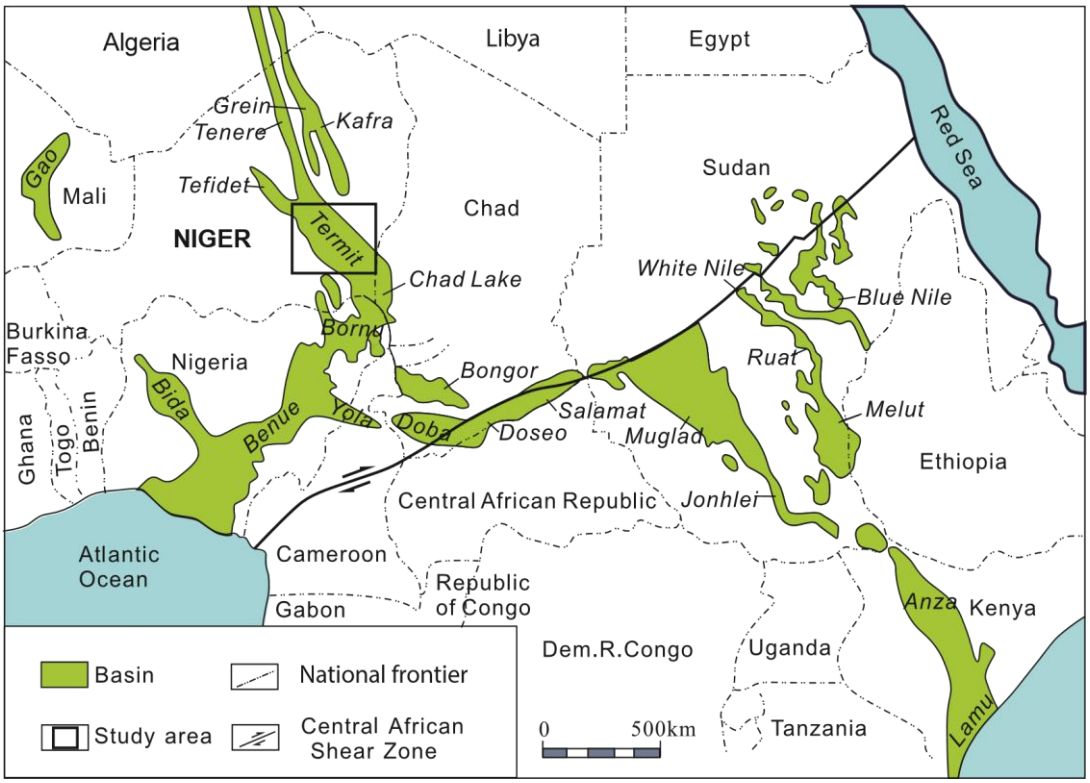

Fig 1: Regional map of West and Central African rift system with location of Termit basin in Eastern Niger [27]

2.2 Samples

The samples from clayey oil source rocks were taken at the Centre de Documentation et d'Archives Pétrolières du Niger (CDP). These are cuttings from Yg and Dg formations at intervals of 2507 to 3025 m and 3025 to 3325 m from F-1AT well for the X = 519535, 254 m Eastern and Y = 1766538.873 m Northern coordinates.

2.3 Methods

The drilling cuttings samples were washed to remove them from the drilling mud. Several analyses were conducted to characterize these samples. These are X-ray diffraction (XRD), X-ray fluorescence spectrometry (XRF), infrared spectroscopy (IR), scanning electron microscopy combined with energy dispersive spectrometry (SEM/EDS) and the Brunauer, Emmett and Teller (BET) method.

The XRF was made using portable XRF spectrometer Niton XL3t® type coupled with a computer to ensure the transfer of data after analysis through the NDT (Niton Data Transfer) software.
The measure in All-Geo mode were performed on an accessory equipped with an RFID (Radio Frequency Identification) chip allowing the analyzer to automatically detect and convert it into a benchtop analyzer. Thus, the elemental composition of crude rock samples was determined.
For the XRD analysis, the crude rock samples were analyzed firstly on disoriented powder and then prepared according to Medard protocol [28]. The oriented section of clayey fractions (less than 2µm) obtained were made and previously analysed in order to be saturated with ethylene glycol and heated to 550°C. The diffractograms are obtained by using a Bruker D8 ADVANCE diffractometer in θ/2θ mode. The relative percentage of each clay phase was determined by using the FITYK diffractogram processing software and Thorez intensity correction factor [29–31]. This analysis made it possible to determine mineral composition of the crude rock samples and to identify different crystalline phases contained in clayey fractions. Then, the crude rock samples were analyzed by using a Bruker FT-IR spectrometer equipped with a diamond crystal in 400 to 4000 cm^{-1} wavelength range. This analysis allowed to determine the different functions that are characteristics of crystalline phases through their vibration modes. The Brunauer, Emmett and Teller (BET) method was used to estimate the specific surface area of crude rock samples.
At the end, scanning electron microscopy coupled with energy dispersive spectrometry (SEM/EDS) made it possible to study the morphology of minerals through digital images and to determine the distribution of elements in minerals and the relative content at a given point in the images.
The device used is a SEM/EDS with Variable Pressure of the D.C.A.R. (MEB FEG Supra 40 VP Zeiss), equipped with an X-ray detector (OXFORD Instruments X-Max 20) connected to an EDS (Inca Dry Cool, without liquid nitrogen) microanalyst platform.

3. Results and discussion

3.1 X-ray diffraction

The mineralogical composition of the crude rock samples determined by the X-ray diffraction and performed on disoriented powder is shown in Table I.

Table I: Mineralogical composition of crude rock samples

Samples	**Samples Constituents of crude rock (%) (**%)							
	Quartz	Muscovite	Garnet	Siderite	Pyrite	Clays	Aragonite	Albite
Dg	25,20	5,00	1,10	3,20	12,80	52,80	0,00	0,00
Yg	32,60	8,40	0,00	0,00	7,00	42,70	5,20	3,00

This table shows a dominance of clays in both samples (52.8% for Dg and 42.7% for Yg). These samples contain quartz, pyrite and muscovite in significant proportions. In some samples, minerals such as siderite, albite, aragonite and garnet are found secondarily. The presence of pyrite in these clays samples is subject to shrinkage and swelling for the rocks studied [32]. Figure 2 shows the diffractograms of the crude rock samples from Dg and Yg formations. Peaks can be observed which also have the characteristics of quartz, kaolinite and illite [28, 33–36]. For clayey fractions, mineralogy presents two types of clayey minerals: the simple mineral, which is kaolinite in a very large proportion in the two samples, and interstratified minerals with two and three different sheets also composed of two types of regular and irregular edifices [37, 38] (Table II and Figure 3). The presence of these interstratified compounds of type 2:1 minerals confirms the relative abundance of potassium and calcium in samples

and possible intrastructural substitutions [39, 40]. These interstratified minerals, in particular illite-smectite and illite-smectite-chlorite, have a high swelling potential [32, 41]. Figure 3 shows the XRD diffractograms of the clayey fractions of Dg and Yg formations.

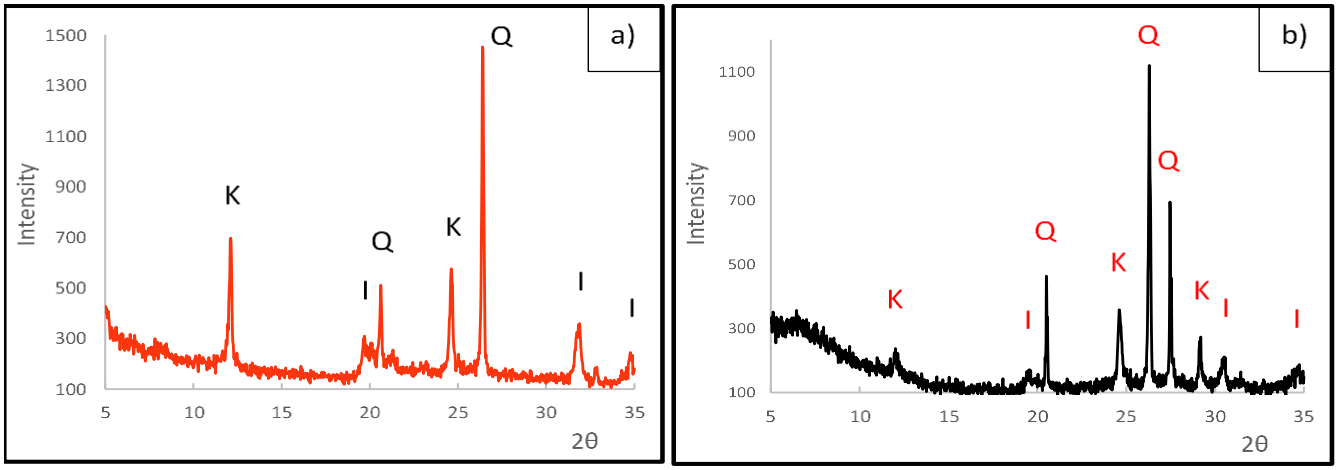

Figure 2: XRD diffractograms of the crude samples a) Dg formation and b) Yg formation; K: kaolinite; I: Illite Q: Quartz.

Table II: Mineralogical composition of the clayey fractions of Dg and Yg formations.

Samples	Single	Regular interstratified	Irregular interstratified	
	Kaolinite	Illite-smectite	Chlorite-illite	Illite-smectite-chlorite
Dg	51.00	31.40	17.60	0
Yg	67.90	0	0	32.10

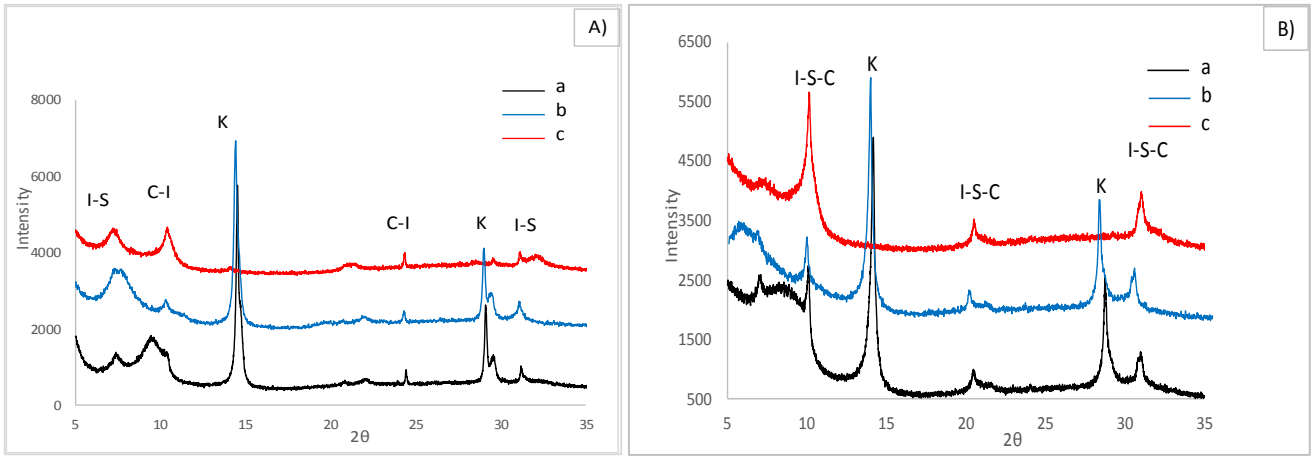

Figure 3: XRD diffractograms of the clayey fractions of A) Dg and B) Yg; a: natural; b: ethylene glycol; c: heated to 550°C; K: kaolinite; C-I: Chlorite-Illite; I-S : Smectite-Illite; I-S-C: Illite-Smectite-Chlorite.

3.2 X-ray fluorescence

The XRF results are presented in Table III. Here, the abundance of silicon and aluminum on one hand and the relatively high Si/Al ratios on the other hand in the XRF elemental analysis results confirm the clay and quartz content of the crude rocks. The high iron content also confirms the presence of pyrite in the crude samples. The relatively high contents of potassium (K) and calcium (Ca) are probably due to substitutions in the octahedral and tetrahedral structures of Al^{3+} by Fe^{2+} and Si^{4+} by Al^{3+} or Fe^{3+} respectively, thus causing a slight charge deficit in these structures and compensated by these interlayer cations in clay materials [37, 42]. This is due to the presence of muscovite and probably that of illite and smectite [42].

Table III: Elemental analysis by X-rays fluorescence spectrometry of crude rocks Dg and Yg

Samples	Components of crude rocks (%)									
	Fe	Mn	Ti	Ca	K	S	Mg	Al	Si	SI/Al
Dg	19.1	0.28	1.4	4.31	3.85	2.26	2.08	17.71	48.02	2.71
Yg	13.25	0.09	1.18	4.3	5	1.91	1.6	14.21	57.37	4.04

3.3 Infrared Spectroscopy

Figure 4 shows the IR spectra of the crude rock samples: Dg and Yg. These spectra show absorbance (arbitrary unit) as a function of waves number (cm^{-1}).

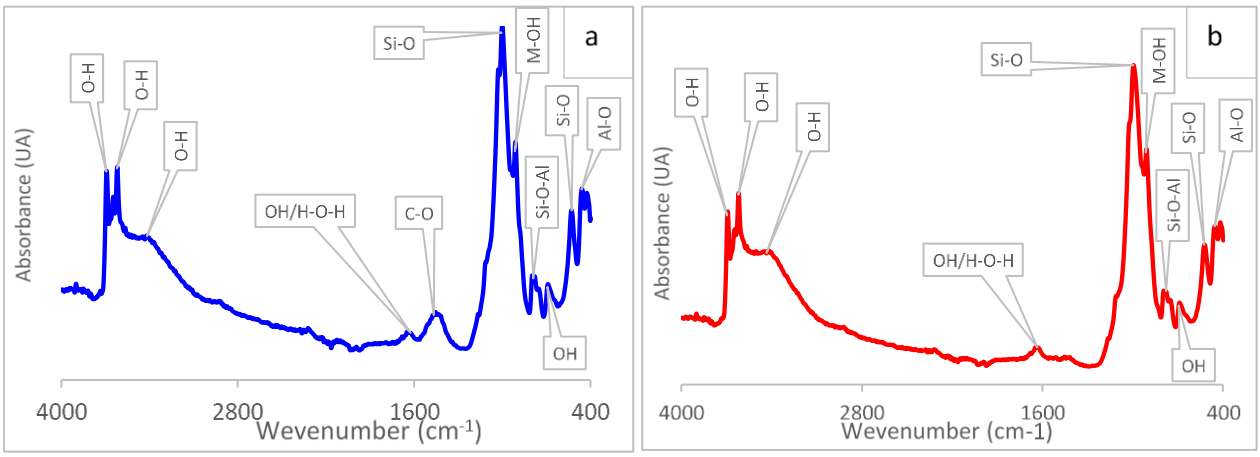

Figure 4: IR spectra of the crude rock samples: a) Dg and b) Yg

The appearance of these spectra is almost identical. The differences observed in shape and position of the absorption bands and peaks can be related to difference in the stacking of the various layers of sheet minerals (clayey minerals). The spectra are characterized by a strong and wide band centered on 1004.3 and 998.2 cm^{-1} corresponding to the Si-O elongation vibration mode of kaolinite [43–47]. Moderately intense lines at 459-461 and 526.7-528.7 cm^{-1} respectively characterize the elongation vibrations of Al-O (illite) and Si-O (smectite) deformation [21]. In addition, there are the bands at 694.1 and 698.1 cm^{-1} respectively, which characterize the hydroxyl (OH) deformation vibration in trioctahedral clay minerals in general. However, fine and low intensity lines with a wave number of 790 cm^{-1} are due to quartz [25, 48]. Similarly, the shoulders around 914.5 and 910.4 cm^{-1} observed for each sample are result of M^{VI}-OH low-precision deflection vibration modes characteristic of montmorillonite (Al, Fe, Mg) [49, 50]. The band centered at 1465.7 cm^{-1} moderately thick of C-0 elongation vibration corresponds to the presence of calcium carbonate ($CaCO_3$) [25, 51]. The bands of H-O elongation and H-O-H deformation vibration modes in water molecules absorbed or present in the cavities of the structure of clay materials are observable at 1624.9 and 1647.4 cm^{-1} [52]. The wide bands and low-intense centered at 3417.2 and 3423.4 cm^{-1} respectively are due to the symmetric and asymmetric elongation vibration modes of OH for water adsorbed or interspersed in the interlayer space. The less intense lines at 3212.4 and 323.4 cm-1 and then at 3692.8 and 3694.9 cm-1 correspond to region of structural OH elongation modes in the octahedral layer characteristic of kaolinite [43, 47, 53]. The absorption bands observed for Dg and Yg (Figure 5) are well related to the characteristic bonds of clay minerals of type 1:1 (Kaolinite), type 2:1

(smectite and Illite), quartz and carbonate (Dg). These results, therefore, confirm those found by the DRX and FRX. The specific surface areas of Dg and Yg samples for this study are 530.40m2/g and 464.90m2/g respectively. These relatively large values give these samples a high swelling potential [32].

3.4 Scanning Electron Microscopy / Energy Dispersion Spectrometry

Figure 6 shows detrital quartz grains (Q) embedded in a clayey paste and covered with illitic materials (I), sometimes chloritic (C) and interstratified illite-smectite (I-S) (Fig. 5-(a)). The pores between quartz grains are partially filled with pseudo-hexagonal kaolinite and interstratified illite-smectite (I-S) and chlorite-smectite (C-S) (Fig. 5-(a), (d) and Fig. 6-(a), (b)) [54, 55]. Books of kaolinite, fan chlorites and micropores are also found in pore fillings (Fig. 5-(b) and (d)) [55].

Micrographs in figure 5 (c) and (d) and figure 6 (a) and (b) show that clayey particles form irregularly contoured blocks and sheets and some aggregate clusters due to other associated minerals. This morphology is characteristic of kaolinite poorly crystallized [48, 54, 55]. Indeed, these results are in agreement with the XRD, XRF and IR analyses. The energy dispersive spectrum of samples in Figure 6 - (c) and (d) shows that the majority peaks of the elements observed in these spectra are common elements observed using XRD and XRF [55]. These are silicon (Si), aluminum (Al), magnesium (Mg), iron (Fe), sodium (Na), potassium (K), calcium (Ca), titanium (Ti) and sulphur (S). The Au and C elements come from the support grid and sample cap. The chemical composition of crude rocks expressed as oxides of these elements is presented in Table IV.

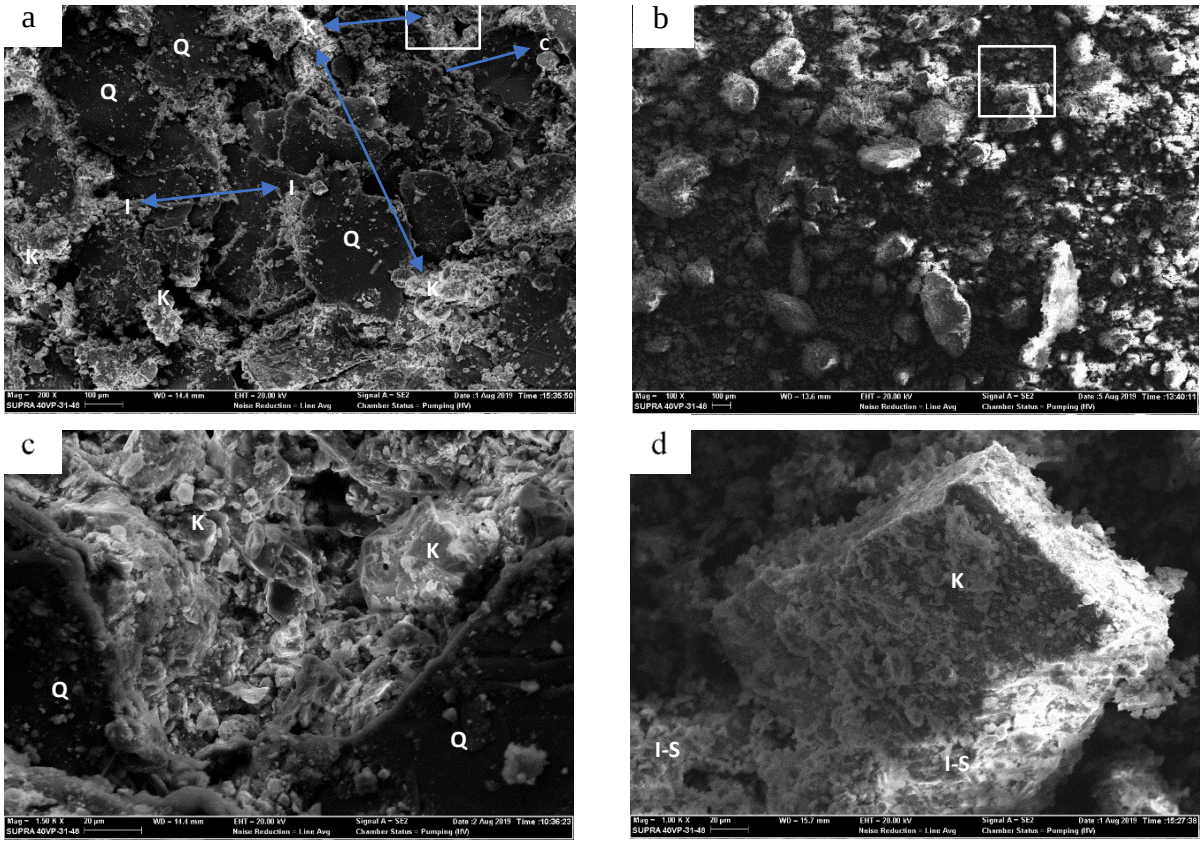

Figure 6: SEM images of crude rocks: (a) - Yg sample at 100µ; (b) - Dg sample at 100µ; (c) - Yg sample at 20µ and (d) - Dg sample at 20µ

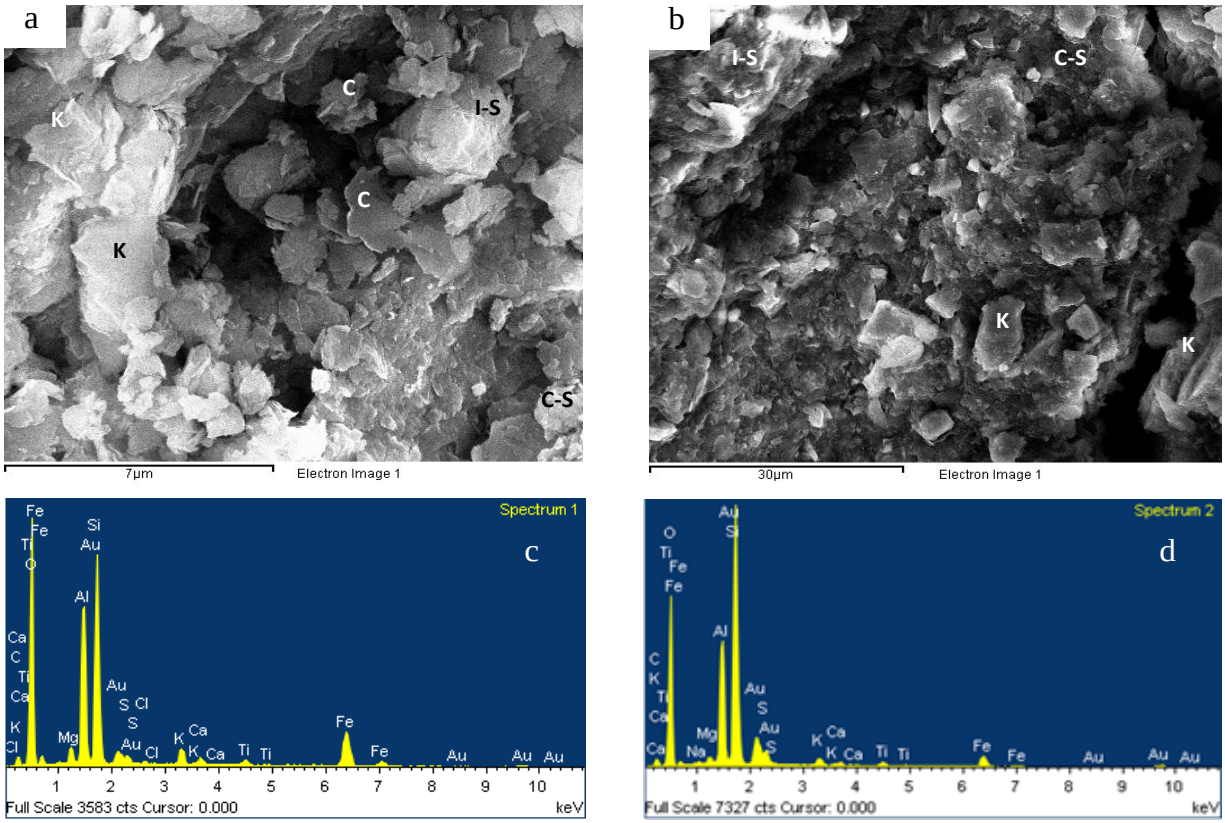

Figure 7: SEM images and corresponding EDS spectra of the crude rock samples: (a) - Yg sample at 7µ; (b) - Dg sample at 30 µ; (c) - Yg spectrum and (d) - Dg spectrum.

Table V: Chemical composition of crude rocks (Yg and Dg)

Oxides	**Na_2O**	**MgO**	**Al_2O_3**	**SiO_2**	**SO_3**	**K_2O**	**CaO**	**TiO_2**	**FeO**	**SiO_2/ Al_2O_3**
Dg (c) (%)	1.67	1.39	18.87	52.93	0	3.01	5.11	1.78	12.03	2.80
Yg (d) (%)	0.00	2.00	21.05	50.32	1.89	3.22	4.99	1.29	13.37	2.39

The EDS analysis (Table IV) shows SiO_2 / Al_2O_3 ratio values of 2.39 and 2.80 respectively for Yg and Dg are significantly higher than those of standard kaolinite which are 1.73 to 1.8 [54, 56]. This is in concordance with the results of the XRD and XRF which reveal the presence of siliceous minerals, in particular quartz and small amounts of type 2:1 clay, such as smectite and illite in crude rocks [57]. Therefore, the mineralogical composition of the Dg and Yg raw rocks and their clayey fractions, and their specific surface areas show that these rocks present a risk of swelling that can cause the jamming of the drilling rig and the drilling bit.

Conclusion

Dg and Yg source rocks are mainly composed of clay (52.80 and 42.70%) and quartz (25.20 and 32.60%) respectively. These rocks also contain minerals such as muscovite (5.00% for Dg and 8.84% for Yg) and pyrite (12.80% for Dg and 7.00% for Yg) with significant proportions. The clayey fractions (< 2 µm) of Dg and Yg are mainly dominated by kaolinite (51.00% and 67.9%). In addition, Dg clayey fraction contains interstratified with two different sheets which are illite-smectite (31.40%) and illite-chlorite

(17.60%) and Yg clayey fraction of interstratified with three different sheets which is illite-smectite-chlorite (32.10%). Finally, the crude rocks are characterized by relatively high specific surface areas (530.40m2/g for Dg and 464.90m2/g for Yg). Thus, the presence of significant proportions of pyrite, interstratified minerals illite-smectite and illite-smectite-chlorite as well as relatively high specific surface areas, give these rocks a risk of swelling. It is therefore important to conduct a study on the swelling potential of these rocks to assess the rate of relative swelling to the type of drilling fluid used to limit the risk of jamming of the drilling rig and the drilling bit.

References

1. M. Zanguina, A. Bruneton, R. Gonnard, « An Introduction to the Petroleum Potential of Niger », *J. Pet. Geol.*, 21(1) (1998) 83-103.
2. B. Liu, L. Wan, F. Mao, J. Liu, M. Lü, et Y. Wang, « Hydrocarbon potential of upper cretaceous marine source rocks in the Termit basin, Niger », *J. Pet. Geol.*, 38 (2) (2015) 157-175.
3. M. Harouna et P. Philp, « Potential petroleum source rocks in the Termit Basin, Niger », *J. Pet. Geol.*, vol. 35, (2012) 165–185. DOI: 10.1111/j.1747-5457.2012.00524.x.
4. M. Harouna, J. D. Pigott, et R. P. Philp, « Burial history and thermal maturity evolution of the Termit basin, Niger », *J. Pet. Geol.* 40, (2017) 277–297. https://doi.org/10.1111/jpg.12676.
5. H. Lai *et al.*, « Organic geochemical characteristics and depositional models of Upper Cretaceous marine source rocks in the Termit Basin, Niger », *Palaeogeogr. Palaeoclimatol. Palaeoecol.*, 495 (2018) 292-308. https://doi.org/10.1016/j.palaeo.2018.01.024.
6. L. Wan, J. Liu, F. Mao, M. Lv, et B. Liu, « The petroleum geochemistry of the Termit Basin, Eastern Niger », *Mar. Pet. Geol.*, 51 (2014) 167-183.
7. H. Xiao *et al.*, « Geochemical characteristics of Cretaceous Yogou Formation source rocks and oil-source correlation within a sequence stratigraphic framework in the Termit Basin, Niger », *J. Pet. Sci. Eng.*, 172 (2019) 360-372. https://doi.org/10.1016/j.petrol.2018.09.082.
8. H. Faure et M. Niger, « Reconnaissance géologique des formations sédimentaires post-paléozoïques du Niger oriental" et traités dans leur ouvrage “Géologie du Niger” », Numéro OCLC 490477133 (1966).
9. G. J. Genik, «Regional framework, structural and petroleum aspects of rift basins in Niger, Chad and the Central African Republic (C.A.R.)», *Tectonophysics*, 213 (1992) 169-185. https://doi.org/10.1016/0040-1951(92)90257-7.
10. E. Chang et L. S. Zung, « 3D Reservoir Characterization of Field Deta, Termit Basin, Niger », in *ICIPEG* , 10 (2017) 323-335. DOI: 10.1007/978-981-10-3650-7_28.
11. B. Liu, G. Zhang, F. Mao, J. Liu, D. Cheng, et M. Lü, « The petroleum system of the Tenere Basin: oil geochemistry from the SH-1 wildcat well in eastern Niger », *Pet. Geosci.*, 23 (2017) 427-439. **DOI:** https://doi.org/10.1144/petgeo2015-067.
12. B. Liu *et al.*, « Structural evolution and main controlling factors of the Paleogene hydrocarbon accumulation in Termit Basin, eastern Niger », *Shiyou XuebaoActa Pet. Sin.*, 33 (2012) 394-403.
13. Z. M. Muhammad Syafiq, Z. Lo Shyh, et M. R. Abdul Ghani, « Petrophysical Analysis on Radioactive Sands for Koala Field in Termit Basin, Niger », *J. Eng. Appl. Sci.*, 13 (2018) 5122-5130. DOI: 10.36478/jeasci.2018.5122.5130.
14. M. N. Nasaruddin, L. S. Zung, et A. G. M. Rafek, « Petrophysical Analysis of E5 sand group of Sokor Formation, Termit Basin, Niger », *IOP Conf. Ser. Earth Environ. Sci.*, 88 (1) (2017) 012003. DOI: 10.1088/1755-1315/88/1/012003.

15. Z. Ning, G. Xia, H. Jiangqin, C. Zhongmin, et Z. Guangya, « Sedimentary Characteristics and Lithological Trap Identification of Distant Braided Delta Deposits: A Case on Upper Cretaceous Yogou Formation of Termit Basin, Niger », *E3S Web Conf.*, 53 (1) (2018) 03020.
16. X. Wang *et al.*, « Controlling factors and accumulation model of hydrocarbon reservoirs in the Upper Cretaceous Yogou Formation, Koulele Area, Termit Basin, Niger », *J. Earth Sci.*, vol. 28 nº 6, (2017) 1126-1134. https://doi.org/10.1007/s12583-016-0936-5.
17. L. Zhou *et al.*, « Controlling factors of hydrocarbon accumulation in Termit rift superimposed basin, Niger », *Pet. Explor. Dev.*, 44 nº 3 (2017) 358-367
18. « "Grim. R. E., Clay Mineralogy, 2nd ed. McGraw-Hill, New York (, R. E, R. E" на Поиске Mail.Ru » ISBN: 0070248362 9780070248366 (1968).
19. D. M. Moore et R. C. Reynolds, *X-ray diffraction and the identification and analysis of clay minerals*. Oxford University Press, ISBN: 019505170X, 9780195051704 (1989).
20. F. Bergaya et G. Lagaly, « Chapter 1 General Introduction: Clays, Clay Minerals, and Clay Science », in *Developments in Clay Science*, vol. 1, F. Bergaya, B. K. G. Theng, et G. Lagaly, Éd. Elsevier, 1 (2006) 1-18. https://doi.org/10.1016/S1572-4352(05)01001-9.
21. M. Floarea, T. Michel, et A. Lazar, « Analyse de certains minéraux argileux utilises a la préparation des fluides de forage écologiques », présenté à Quatrième Colloque Franco-Roumain de Chimie Appliquée, France, 5 N°3 (2006) 8.
22. D. M. Moore et R. C. Reynolds, *X-ray Diffraction and the Identification and Analysis of Clay Minerals*, Oxford University Press Oxford, ISBN: 978-0-19-505170-4 (1989).
23. Z. Yigzaw, « Analyse des processus de retrait-gonflement de sols argileux en réponse à des sollicitations hydriques cycliques : rôle de la microstructure », PhD Thesis, Paris, ENMP, (2009).
24. M. J. Collins, A. N. Bishop, et P. Farrimond, « Sorption by mineral surfaces: Rebirth of the classical condensation pathway for kerogen formation? », *Geochimica et Cosmochimica*, Acta, 59 N°11 (1995) 2387-239.
25. T. Camille, « Caractérisation et quantification des minéraux argileux dans les sols expansifs par spectroscopie infrarouge aux échelles du laboratoire et du terrain. », PhD Thesis, Université Toulouse 3 Paul Sabatier, (2010).
26. N. Jean Paul, « Techniques d'exploitation pétrolière : Le Forage ». (Français). *Institut français du pétrole*, ISBN: 978-2-7108-0558-8 (1993).
27. M. Harouna, J. D. Pigott, et R. P. Philp, « Burial History and Thermal Maturity Evolution of the Termit Basin, Niger », *J. Pet. Geol.*, 40 nº 3 (2017) 277-297.
28. T. Médard, N. Carrillo, C. Franke, et N. Martineau, *Technique de préparation des minéraux argileux en vue de l'analyse par diffraction des Rayons X et introduction à l'interprétation des diagrammes*. 3 (2013) 34.
29. P. E. Biscaye, « Mineralogy and Sedimentation of Recent Deep-Sea Clay in the Atlantic Ocean and Adjacent Seas and Oceans », *GSA Bull.*, 76 nº 7 (1965) 803-832.
30. P. E. Biscaye, « Distinction between kaolinite and chlorite in recent sediments by x-ray diffraction », *Am. Mineral.*, 49 nº 9-10 (1964) 1281-1289.
31. J. Thorez J., *Practical identification of clay mineral, À handbook for teachers and students in clay mineralogy*, G, Lelotte, Dison. Belgique, Numéro OCLC: 2558848 (1976).
32. M. Audiguier, Z. Geremew, S. Laribi, et R. Cojean, « Caractérisation au laboratoire de la sensibilité au retrait-gonflement des sols argileux », *Rev. Fr. Géotechnique*, nº 120-121 (2007) 67-82. https://doi.org/10.1051/geotech/2007120067.

33. M. Raven et P. Self, « Identification and Quantification of Clays », *Clays in the Minerals Processing Value Chain*, (2017) 142-204.
34. Hillier, S. « Quantitative analysis of clay and other minerals in sandstones by X-ray powder diffraction (XRPD). » Clay mineral cements in sandstones (1999) 213-251.
35. G. Brown et G. W. Brindley, « X-ray diffraction procedures for clay minerals identification », *Crystal Structures of Clay Minerals and their X-ray Identification*, Mineralogical Society (London), (1980) 305– 360.
36. G. W. Brindley et G. Brown, Éd., *Crystal Structures of Clay Minerals and their X-Ray Identification*. Colchester and London: Mineralogical Society of Great Britain and Ireland, ISBN: 978-0-903056-08-3 978-0-903056-37-3 (1980).
37. J. Lucas, N. Trauth, et M. Thiry, « Les minéraux argileux des sédiments paléogènes du Bassin de Paris. Evolution des smectites et des interstratifiés (7-14Sm) », *Bull. Groupe Fr. Argiles*, 26 n° 2 (1974) 245-262.
38 D. M. C. Mac Ewan, « Some Notes on the Recording and Interpretation of X-Ray Diagrams of Soil Clays », *J. Soil Sci.*, 1 n° 1 (1950) 90-103. https://doi.org/10.1111/j.1365-2389.1950.tb00721.x.
39. L. Pauling, « The Structure of the Micas and Related Minerals », *Proc. Natl. Acad. Sci.*, 16 n° 2 (1930) 123-129. https://doi.org/10.1073/pnas.16.2.123.
40. L. Pauling, « THE STRUCTURE OF THE CHLORITES », *Proc. Natl. Acad. Sci. U. S. A.*, 16 n° 9 (1930) 578-582. doi: 10.1073/pnas.16.9.578.
41. G. Montes Hernandez, « Experimental study of water adsorption and swelling of clays by Environmental Scannig Electron Microscopy (ESEM) and digital image analysis », Theses, Université Louis Pasteur - Strasbourg I, (2002).
42. J. Lucas, *La transformation des minéraux argileux dans la sédimentation. Études sur les argiles du trias*. Persée - Portail des revues scientifiques en SHS, 23 (1962) 197.
43. A. K. Chakraborty, *Phase Transformation of Kaolinite Clay*. Springer India, ISBN: 978-81-322-1153-2 (2014). DOI 10.1007/978-81-322-1154-9.
44. V. C. Farmer, Éd., « Vibrational Spectroscopy in Mineral Chemistry », in *The Infrared Spectra of Minerals*, Londan: Mineralogical Society of Great Britain and Ireland, (1974) 1-10.
45. V. C. Farmer, Éd., « The Layer Silicates », in *The Infrared Spectra of Minerals*, Londan: Mineralogical Society of Great Britain and Ireland, 1974, p. 331-363.
46. V. C. Farmer, Éd., *The Infrared Spectra of Minerals*. Londan: Mineralogical Society of Great Britain and Ireland, ISPN: 978-0-903056-05-2 978-0-903056-53-3 (1974).
47. C. Ibtissem, L. Bachir, B. Lakhdar, C. Abdelmadjid, F. Natalie, « Caractérisation minéralogique et physico-chimique des formations argileuses sous numidiennes de la région d'Azzaba (NE Algérie)», *Courrier du Savoir* 26 (2018) 621-632.
48. A. Qlihaa, S. Dhimni, F. Melrhaka, N. Hajjaji, et A. Srhiri, « Caractérisation physico-chimique d'une argile Marocaine [Physico-chemical characterization of a morrocan clay]», *J. Mater. Environ. Sci*, 7 (2016) 1741-1750.
49. M. Pelletier, « Application de la spectroscopie infrarouge à l'étude de l'organisation de l'eau aux interfaces : le cas des phyllosilicates 2:1 », (1999).
50. G. Marou, Z. Adamou, N. Ibrahim, et B. Anne, « Caracterisation d'une argile mixte du Niger », *Rev. CAMES – Sciences Struct. Mat.* 1 (2013) 11.
51. A. S. Benosman, H. Taibi, M. Mouli, et M. Belbachir, « Valorisation de la spectrométrie infrarouge (irtf) pour l'analyse qualitative de composes des ciments, argiles, et des mélanges ciment/argile », *Communication Sciences & Technologie* N°3 (2004) 77-88.

52. T. N. Leonel, « Memoire Online - Comportement thermique des géopolymères obtenus à partir d'une argile kaolinite - Leonel Tchadjie Noumbissie », *Memoire Online*, (2012).
53. J. Chaussidon et R. Prost, « Spectre infrarouge des vibrations de valence de l'eau adsorbée par la montmorillonite », *Bull. Groupe Fr. Argiles*, 19 N° 2 (1967) 25-38.
54. H. H. Murray, *Applied Clay Mineralogy: Occurrences, Processing and Applications of Kaolins, Bentonites, Palygorskitesepiolite, and Common Clays*, 2nd edition. Amsterdam; Boston: Elsevier Science, ISBN: 978-0-444-51701-2 (2006).
55. J. E. Welton, *Sem Petrology Atlas*. Tulsa, Okla: Amer Assn of Petroleum Geologists, (1984).
56. Z. Ousman, A. Alassane, L. N. Dan, R. Paolo, T. P. Gemma, et A. Issaka, « Caractérisation des Sols de Périmètres Irrigués de l'Ouest du Niger par Diffraction de Rayons X, *J. Soc; Ouest-Afr. Chim*. 026 (2008) 89 - 97.
57. C. A. Jouenne, *Traité de Céramiques et Matériaux Minéraux*, Editions Septima. Paris, ISBN: 5552904845010 (1990).

(2020) ; http://www.jmaterenvironsci.com